

## **FEM MODELING ON THE COMPACTION OF Fe AND Al COMPOSITE POWDERS**

**P. Han, X. Z. An\*, Y. X. Zhang, Z. S. Zou**

School of Materials and Metallurgy, Northeastern University, Shenyang, China

*(Received 10 February 2015; accepted 30 April 2015)*

### **Abstract**

*The compaction process of Fe and Al composite powders subjected to single action die compaction was numerically modeled by FEM method. The relationship between the overall relative density and compaction pressure of the compacts with various Al contents was firstly identified, and the influences of Al content on the local relative density, stress, and their distributions were studied. Then the compaction pressure effects on the above properties with fixed Al content were discussed. Furthermore, detailed flow behaviors of the composite powders during compaction and the relationship between the compaction pressure and the ejection force/spring back of the compact were analyzed. The results show that: (1) With each compaction pressure, higher relative density can be realized with the increase of Al content and the relative density distribution tends to be uniform; (2) When the Al content is fixed, higher compaction pressure can lead to composite compact with higher relative density, and the equivalent Von Mises stress in the central part of the compact increases gradually; (3) Convective flow occurs at the top and bottom parts of the compact close to the die wall, each indicates a different flow behavior; (4) The larger the compaction pressure for each case, the higher the residual elasticity, and the larger the ejection force needed.*

*Keywords: FEM modeling, Fe and Al composite powders, compaction, powder metallurgy*

### **1. Introduction**

Porous materials have been widely applied in many industries such as aeronautics and aerospace, medical, metallurgy, construction, and mechanics etc. [1]. Among these materials, the Fe-Al intermetallic compounds play the dual role of both structural and functional materials because this porous material not only has superior high temperature oxidation and corrosion resistance of the intermetallic compound, [2] but also exhibits the features of low volume density, high specific surface area and good permeability of porous material. Fe-Al intermetallic compound porous material can work in severe environment, e.g. in high temperature gas dust elimination and liquid filtration [3, 4]. Therefore, many production processes were proposed in this regards, which include metallurgical smelting, casting, rolling, self-propagating synthesis and reaction synthesis etc. [5-10]. Due to the high melting point of Fe-Al intermetallic compound, its production by normal smelting and casting is costly and the corresponding process is relatively complicated. In comparison, the reaction synthesis method in powder metallurgy (PM) has been regarded as an important way in manufacturing high-performance Fe-Al intermetallic compound with low cost. In this process,

the large diffusion coefficient difference between Fe and Al will create strong Kirkendall effects [11], which has been used by Gao et al. in the production of Fe-Al intermetallic compound porous materials using die compaction followed by sintering [12,13]. However, their research was mainly focusing on the sintering stage, much less work was conducted on the compaction stage, which has been regarded as one of the important stages in PM production and its effectiveness has been identified in our previous physical and numerical studies [14, 15]. Basically, a compact with high relative density, uniform density and stress distributions can not only create key effects on the quality and property of the final PM product, but also simplify subsequent process and reduce the cost. Therefore, the research in this stage becomes increasingly important.

In the past decades, people's research interests were gradually transferred to powder cold compaction both physically and numerically. In physical experiments, the work was mainly concentrated on the forming theory and yield criteria [15-22], however, it's really hard to quantitatively characterize the local density distribution, stress distribution, and powder flow behavior in the compact during and after compaction. And the existed geometric nonlinearity, material nonlinearity, and contact nonlinearity all

---

\* Corresponding author: [anxz@mail.neu.edu.cn](mailto:anxz@mail.neu.edu.cn)

increase the experimental difficulties [23-26]. The problem in physical experiments can be overcome by computer numerical simulation, in which the normally used techniques are continuous finite element method (FEM) from macro scale and discrete multi-particle FEM (MPFEM) or discrete element method (DEM) from particulate scale. Zhang et al. carried out MPFEM simulation on the die compaction of Al particles in 2D, where different initial packing structures generated by DEM were considered and the densification behavior and mechanisms were analyzed [27]. Using similar method, Wu et al. modelled the die compaction of Fe and Al powder mixture, where the initial packing structure of Fe and Al particles was ordered [28]. The above modeling can effectively identify the interaction between particles, however, the amount of particles involved is limited due to the large computation capacity needed, which impedes its development in real process. This research barrier can be conquered by traditional FEM from macro scale, therefore, much work was carried out to model the compaction of pure metal powders [29-32]. Recently, the research has been transited to the compaction of composite powders. For example, based on the experimental data from isostatic compaction and die compaction of copper and tungsten composite powders, Kim et al. proposed corresponding numerical simulations [33, 34]. To date, much less work was carried out on the cold compaction of randomly packed Fe and Al composite powders by continuous FEM modeling, especially systematic analysis on the compaction behavior and characterization was lacking.

In this paper, the compaction of Fe and Al composite powders subjected to single action die compaction was numerically simulated by traditional FEM. The relationship between the overall relative density and compaction pressure of compacts with various Al contents was firstly identified, and the influences of Al content on the local relative density, stress, and their distributions were studied. Then the effects of compaction pressure on the above properties with fixed Al content were discussed. Finally, detailed flow behaviors of the composite powders during compaction and the ejection and spring back of the compact were analyzed.

## 2. Numerical method and conditions

### 2.1 Model setup

All the numerical simulations were carried out by using commercialized MSC Marc FEM software, for each case the whole forming process including initial packing in the die, compaction and spring back after ejection was modeled and studied. The modeled composite compact has a cylindrical shape with diameter  $d=20\text{mm}$  and initial packing height

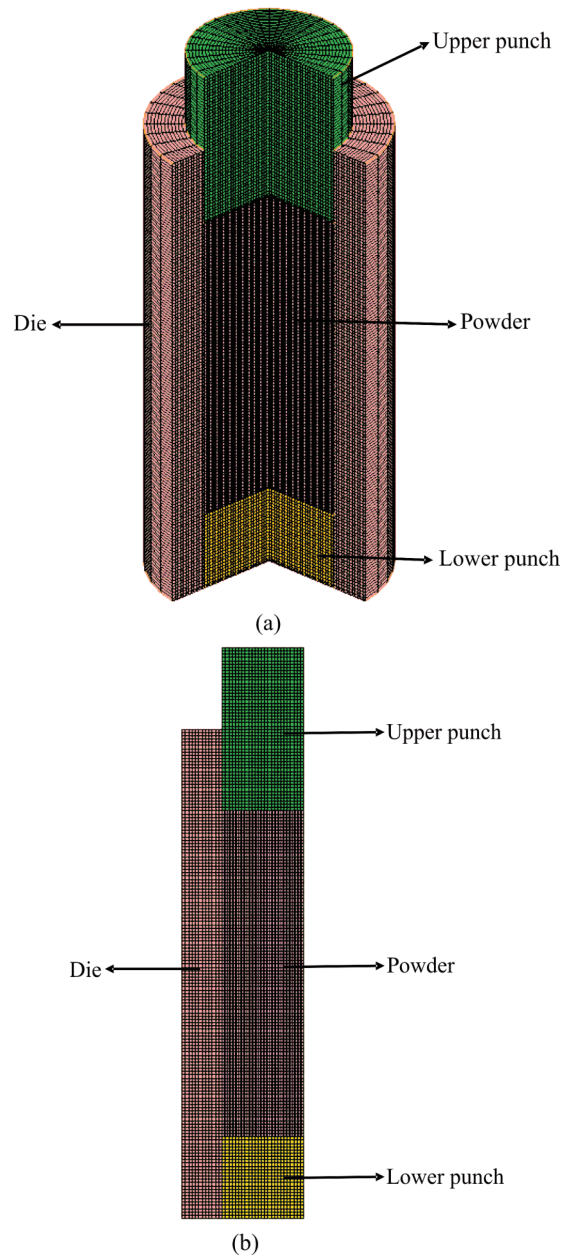


Figure 1. 3D FEM mesh division (a) and corresponding 2D reduced model (b)

$H=40\text{mm}$  which corresponds to the relative density  $\rho=0.62$ . Due to the symmetry of the loading and compact geometry, the 3D FEM mesh division model as shown in Fig. 1(a) is reduced as 2D axial symmetric model (as given in Fig. 1(b)) in the whole computation. During compaction, the modified Shima model was used [19, 20], and the work hardening of the composite powders was incorporated, as given by:

$$F = \frac{1}{\gamma} \left( \frac{3}{2} \sigma^d \sigma^d + \frac{\sigma_m^2}{\beta^2} \right)^{0.5} - \sigma_y$$

where:  $\sigma_y$ -uniaxial yield stress,  $\sigma^d$ -deviatoric stress tensor,  $\sigma_m$ -hydrostatic

stress,  $\gamma$ ,  $\beta$ -materials parameters which are the functions of relative packing density  $\rho$ :  $\gamma=\rho^{2.5}$  and  $\beta=(5.9-5.9\rho)^{-0.514}$ . In simulation, the modified Coulomb friction model was used and the friction coefficient between the powders and the die wall was set to be 0.2. The loading was controlled by the displacement of the upper punch, while the positions of the die wall and the lower punch were fixed.

### 2.2 Simulation parameters

The equivalent Young's modulus of the composite can be calculated by the mixed-mode method, i.e. the upper and lower limits of the Young's modulus of the dense packing body of soft and hard particles can be calculated based on the Voigt equivalent strain assumption and Reuss equivalent stress assumption, respectively [35]. Fe and Al composite powders are also the mixture of hard and soft particles, where large strain of particles can be created during compaction. Therefore the upper limit of the equivalent Young's modulus was used. On other words, the Voigt mixed-mode model was used, and the yield strength of Fe and Al composite compact dense body can be expressed as  $\sigma_c = \sigma_r v_r + \sigma_m v_m$ , where  $\sigma_c$ ,  $\sigma_r$ , and  $\sigma_m$  represent the yield strength of composite powder compact, Fe, and Al, respectively;  $v_r$  and  $v_m$  are the Poisson's ratios of Fe and Al. The Young's modulus of the Fe and Al composite compact dense body is given by  $E_c = E_r v_r + E_m v_m$ , where:  $v_r + v_m = 1$ ,  $E_c$ ,  $E_r$ , and  $E_m$  are the Young's modulus of the composite powder compact, Fe, and Al, respectively. Therefore, the corresponding values for these parameters are  $E_r=120\text{GPa}$ ,  $\sigma_r=120\text{MPa}$ ,  $E_m=62.59\text{GPa}$ , and  $\sigma_r=60\text{MPa}$ .

During compaction, the Young's modulus, Poisson's ratio, and yield strength are all the functions of relative density. Based on the McAdam empirical expression [36] and the assumptions in literature [37-39]. The modified Young's modulus of the composite powder was used in the simulation as  $E=E_c \rho^{3.4}$ . The Poisson's ratio of the composite powder adopted the empirical formula proposed by Zhdanovich as  $\nu=0.5\rho^n$  [40, 41]. According to Kuhn and coworkers' study, for cold compaction  $\sigma=\sigma_c \rho^n$ , where  $n=1.9$  [17].

## 3. Results and discussion

### 3.1 Relationship between overall relative density and compaction pressure P

In a real process, the relationship between the overall relative density  $\rho$  of the compact and the compaction pressure  $P$  is the main concern, which has been modelled and given in Fig. 2. As can be seen, each  $\rho$ - $P$  curve corresponds to a certain Al content and three compaction stages can be identified: (1) low packing density stage. In this stage, the increase of  $\rho$  is not significant and with a low speed when  $P$  is low

(e.g.  $P<20\text{MPa}$ ). The densification mechanism is mainly dominated by particle rearrangement due to the low compaction pressure, and the particles are in jammed state [42]; (2) packing density fast increase stage. With the increase of  $P$ ,  $\rho$  increases abruptly. The densification mechanism is mainly due to the large plastic deformation of particles; (3) high packing density stage. Further increasing  $P$  can lead to much higher packing density, however, the variation rate of  $\rho$  is not as significant as that in stage (2). In this stage, the composite powder compact indicates bulk behavior and only some isolated enclosed voids left inside. The  $\rho$ - $P$  curves in Fig. 2 have similar trends with those results obtained from physical experiments [22] and numerical simulations [28]. Meanwhile, it is also observed that the positions of these  $\rho$ - $P$  curves become higher with the addition of Al powder, but the variation does not change much with the Al powder content due to the not large difference in yielding stage between Fe and Al powders [19].

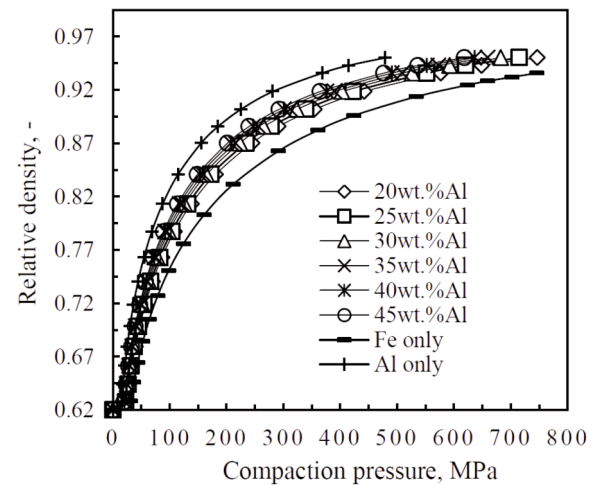


Figure 2. Overall relative density as a function of compaction pressure at various Al contents

### 3.2 Effect of Al powder content

The local relative density distributions in compacts with different Al contents ( $X_{Al}$ ) when  $P=200\text{MPa}$  is shown in Fig. 3. As can be seen, for each Al content the largest and smallest local relative densities distribute at the corner of the compact in contact with the upper and lower punches, respectively. This can be explained by the friction effects between the powder and the die wall. In the other part of the compact, the relative density distribution is relatively uniform at the same height and decreases gradually from the top to the bottom. This result is agreeable with others' physical and numerical results [33]. In addition, the influence of Al content on the local relative density distribution can

also be observed. With the increase of  $X_{Al}$ , the value of the relative density and corresponding distribution area at the upper corner of the compact increases, however, those at the lower corner of the compact decreases. Meanwhile, one can find that increasing  $X_{Al}$  cannot create significant effects on the overall relative density of the compact, which can be identified by the small variation of the height of each compact.

Accordingly, the equivalent Von Mises stress distributions in compacts with various  $X_{Al}$  when  $P=200\text{MPa}$  was analyzed as shown in Fig. 4. Clearly, stress concentration occurs at the upper corner of each compact, which is in accordance with the local relative density distribution in Fig. 3. In comparison, the stress at the lower corner of each compact is very low. The stress distribution in current simulation is in

good agreement with others' research results [43, 44]. At the same time, one can also find that, with the increase of  $X_{Al}$ , the stress domain at the upper corner or at the lower corner does not change much, however, the stress in the central part of each compact decreases, which demonstrates that adding more Al powder will lead to the decrease of overall compact hardness.

### 3.3 Effect of compaction pressure

In addition to the previously discussed influences of Al content on the local relative density and stress distributions in each compact, the effect of compaction pressure was also studied when  $X_{Al}$  is fixed at 25wt.%. In this case, the volume ratio of Al and Fe in the composite powders is approximately

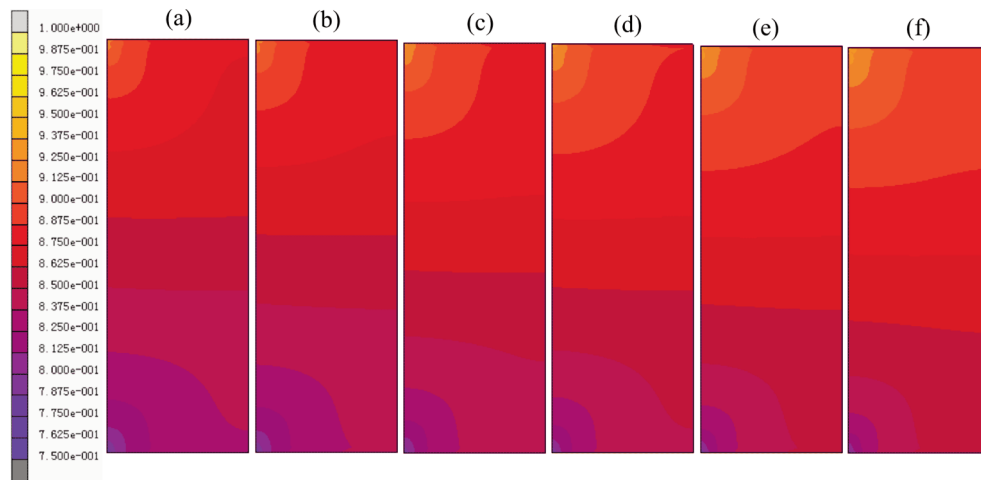


**Figure 3.** Distributions of local relative densities for compacts with various  $X_{Al}$  when  $P=200\text{MPa}$ , where (a)-(f) correspond to  $X_{Al}=20\text{wt.}\%$ ,  $25\text{wt.}\%$ ,  $30\text{wt.}\%$ ,  $35\text{wt.}\%$ ,  $40\text{wt.}\%$ ,  $45\text{wt.}\%$ , respectively

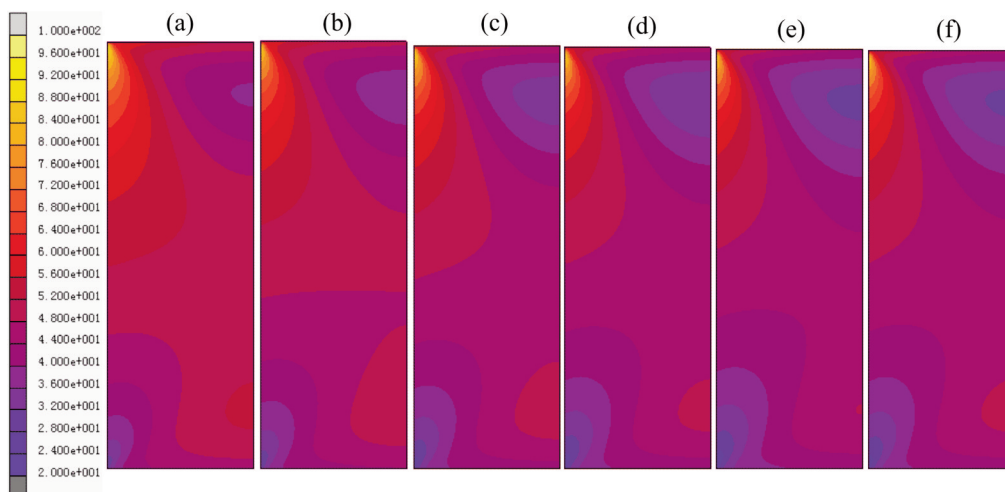


**Figure 4.** Distributions of equivalent Von Mises stress for compacts with various  $X_{Al}$  when  $P=200\text{MPa}$ , where (a)-(f) correspond to  $X_{Al}=20\text{wt.}\%$ ,  $25\text{wt.}\%$ ,  $30\text{wt.}\%$ ,  $35\text{wt.}\%$ ,  $40\text{wt.}\%$ ,  $45\text{wt.}\%$ , respectively

1:1, which is mostly concerned by many researchers [4, 5, 12, 13]. Fig. 5 shows the local relative density distributions in the compacts under different compaction pressures. As seen, in each compact the local relative density distribution has similar trend as that in previous discussion. However, different compaction pressure corresponds to different compaction behaviors. When  $P$  is low, the overall relative density in the compact is low, and the difference between local large  $\rho$  at the upper corner and small  $\rho$  at the lower corner of the compact is significant. With the increase of  $P$ , the overall  $\rho$  increases, and the difference of local relative  $\rho$  becomes less significant.

Fig. 6 gives the equivalent Von Mises stress distributions at various compaction pressures when  $X_{Al}=25\text{wt.}\%$ . One can find that, with the increase of  $P$ ,

the average equivalent Von Mises stress in each compact increases, higher stress (stress concentration) occurs at the upper corner with larger  $P$ , which is in accordance with the local relative density distribution in Fig. 5. Meanwhile, Fig. 6 also shows that a low equivalent Von Mises stress area which locates in the central part (close to the top surface) of the compact appears when  $P$  is increased. This phenomenon is comparable with that in the compaction of alumina agglomerates [43], and the reason may be ascribed to the die wall and the powder flow behavior effect as will be discussed in the following part.

### 3.4 Powder flow behavior during compaction

It is known that the powder movement during compaction is determined by the forces on it. Two

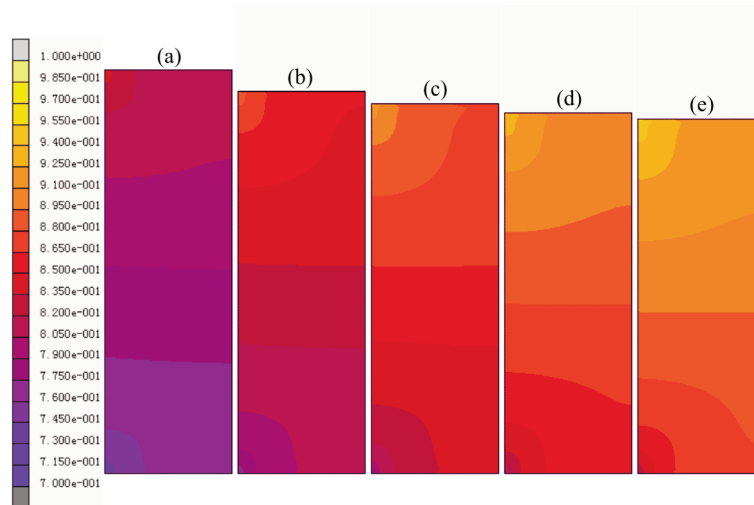


Figure 5. Relative density distributions at various compaction pressures when  $X_{Al}=25\text{wt.}\%$ , where (a)-(e) correspond to  $P=100\text{MPa}$ ,  $150\text{MPa}$ ,  $200\text{MPa}$ ,  $250\text{MPa}$ , and  $300\text{MPa}$ , respectively

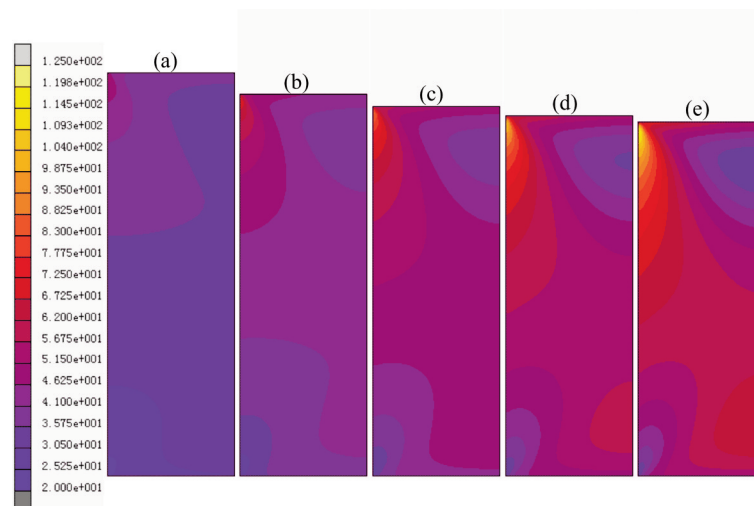


Figure 6. Equivalent Von Mises stress distributions at various compaction pressures when  $X_{Al}=25\text{wt.}\%$ , where (a)-(e) correspond to  $P=100\text{MPa}$ ,  $150\text{MPa}$ ,  $200\text{MPa}$ ,  $250\text{MPa}$ , and  $300\text{MPa}$ , respectively

particle flow behaviors in the die, i.e. flow in axial direction and flow in radial direction, were analyzed in the composite powder compaction. Fig. 7 shows the distribution of axial displacement (a) and its evolution with radial distance at different packing heights (b), where  $P=200\text{MPa}$ ,  $X_{\text{Al}}=25\text{wt.}\%$  and the positions at  $H=4\text{mm}$ ,  $12\text{mm}$ ,  $20\text{mm}$ ,  $28\text{mm}$ , and  $36\text{mm}$  were taken for analysis. Here, the ‘minus’ symbol (-) in front of the displacement means the opposite direction to that of coordinate axis. In the following discussions, the absolute value of displacement is mainly used for convenience. Fig. 7 (a) shows that the powder axial displacement decreases gradually from the top to bottom of the compact. At each height, the axial displacement at the die wall lags behind the central region due to the friction effect between the powder and the die wall. Through the analysis on the axial displacements at different heights as illustrated in Fig. 7 (b), one can find that the axial powder flow at each height has similar trend but different displacement. The closer to the upper punch, the larger the axial displacement.

Accordingly, Fig. 8 displays the radial displacement of the composite powders during compaction, where the positions chosen for analysis were the same as that in Fig. 7. As indicated, convective powder flow can be identified at the top and bottom part of the compact close to the die wall, which is quite different from the axial flow in Fig. 7. Clearly, the powder close to the die wall in the upper

part flows to the center of the compact and that in the lower part flows to the die wall. These phenomena can be demonstrated in Fig. 8 (b), where the curves above and below the horizontal axis which locate in the top and bottom parts in the compact represent the convective flow towards opposite directions. This is because the stress and relative density close to the die wall are relatively high/low in the upper/lower part compared with other parts in the compact (see Figs. 5 and 6), which makes the powder particles in the die wall region flow towards/outwards the central part. While at the middle height of the compact, the convective flow of the composite powder is not significant. And one can also find that, compared with the axial powder displacement, the radial displacement is even smaller.

### 3.5 Ejection and spring back analysis

Compared with the compaction, the ejection of the compact from the die is also an important stage in PM production, which can to some extent determine the product quality and property. Here, the ejection and subsequent spring back of the compacts are analyzed respectively. After unloading, the compact was ejected from the bottom. Fig. 9 provides the equivalent Von Mises stress distributions in the compacts when  $X_{\text{Al}}=25\text{wt.}\%$  and corresponding pressure  $P=100\text{MPa}$ ,  $150\text{MPa}$ ,  $200\text{MPa}$ ,  $250\text{MPa}$ , and  $300\text{MPa}$ . As indicated, the stress is mainly concentrated at the top

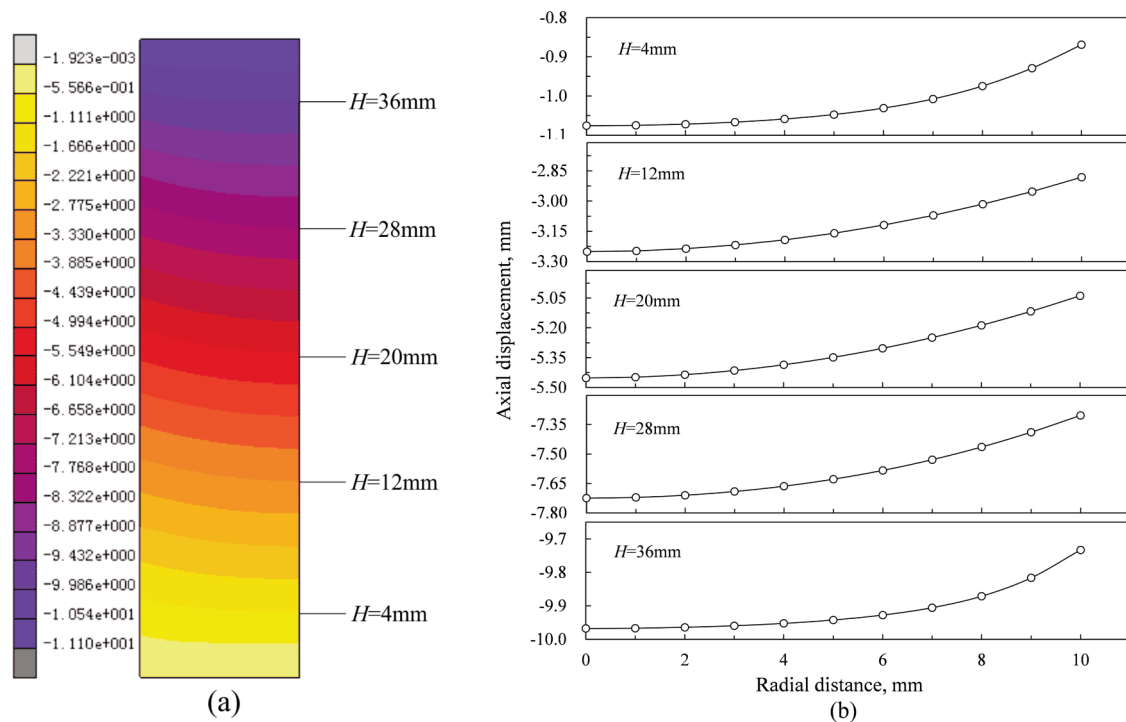


Figure 7. (a) Axial displacement of the powders during compaction; (b) Axial displacements of powder particles at different heights as indicated in (a). Where:  $P=200\text{MPa}$ ,  $X_{\text{Al}}=25\text{wt.}\%$

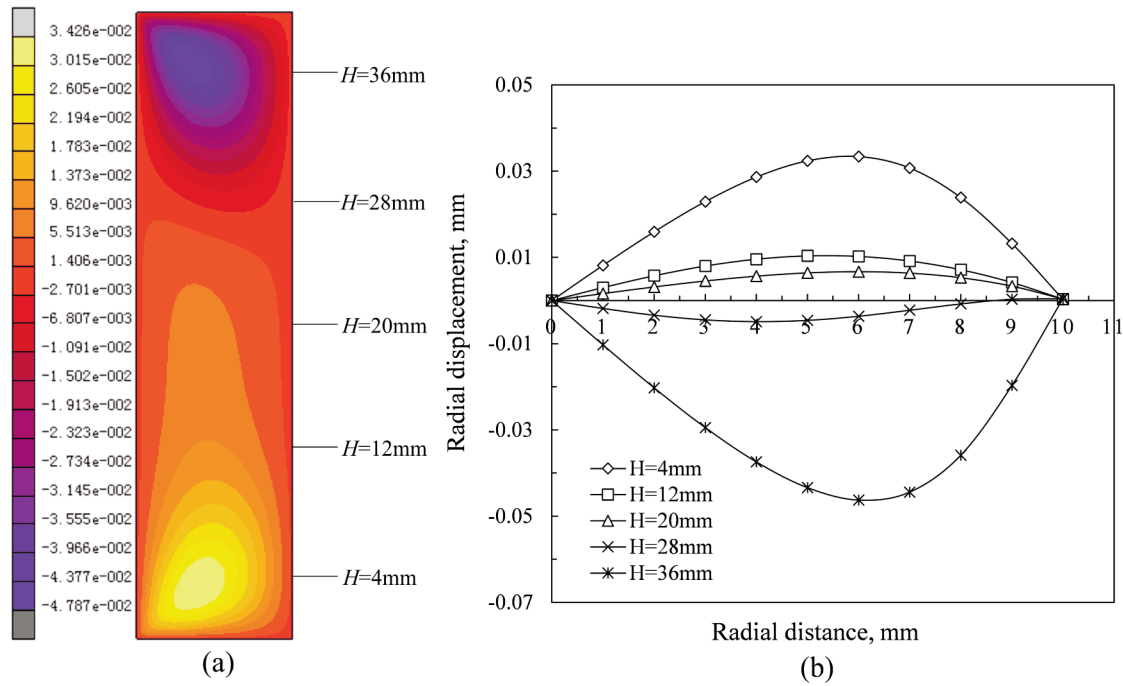


Figure 8. (a) Radial displacement of the powders during compaction; (b) Radial displacement of powder particles at different height as indicated in (a). Where:  $P=200\text{MPa}$ ,  $X_{Al}=25\text{wt.}\%$

corner and central surface of the compact. After unloading, the axial pressure is released, while the radial stress is still restricted by the die wall, which leads to different powder expansion and resultant redistribution. Therefore, the stress concentration formed at these areas will increase the potential of crack formation after ejection, which agrees well with the real process. With the increase of the compaction pressure, the distribution of the equivalent Von Mises stress becomes more non-uniform, which increases the

probability of crack creation and propagation. This is because high compaction pressure will lead to high relative density and small porosity, and the compact indicates bulk behavior which needs to create large stress in the compact to resist the large external pressure. In this case, large stress after ejection is mainly formed at the top, especially at the corner of the compact. Meanwhile, one can also see certain stress at the bottom of the compact, which is due to the bottom ejection effect.

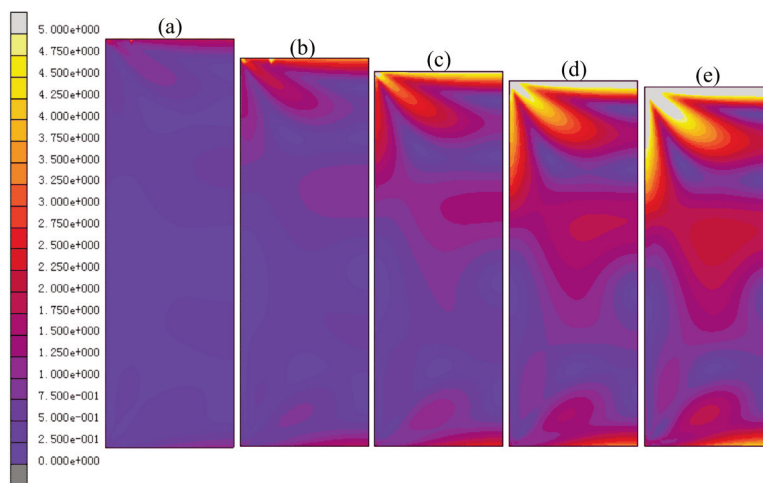
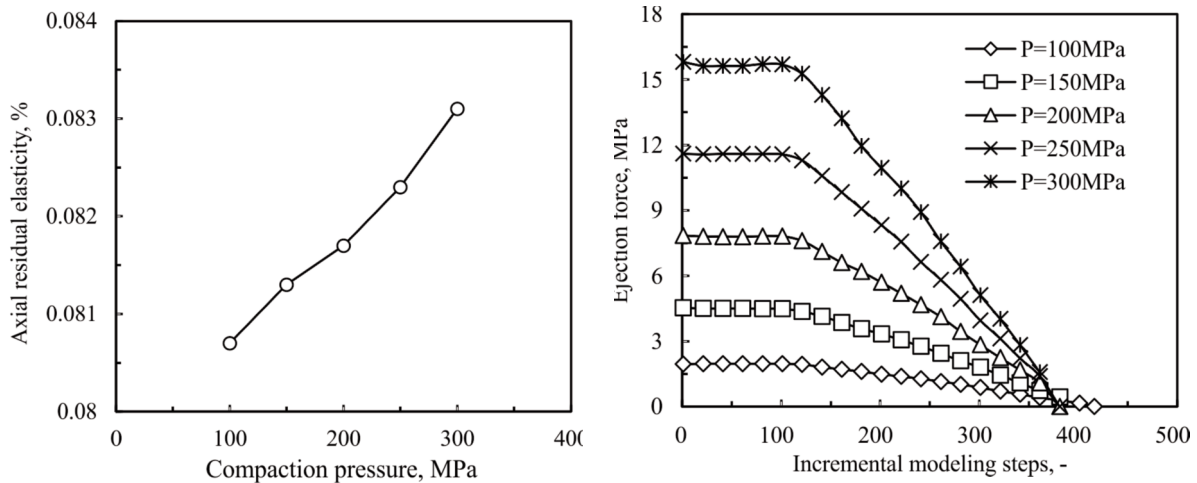


Figure 9. Equivalent Von Mises stress distributions in the compacts after ejection when  $X_{Al}=25\text{wt.}\%$ , where: (a)-(e) correspond to  $P=100\text{MPa}$ ,  $150\text{MPa}$ ,  $200\text{MPa}$ ,  $250\text{MPa}$  and  $300\text{MPa}$ , respectively



**Figure 10.** Evolution of axial residual elasticity with the compaction pressure (a) and ejection force as a function of incremental modeling steps when  $P=100\text{MPa}$ ,  $150\text{MPa}$ ,  $200\text{MPa}$ ,  $250\text{MPa}$ ,  $300\text{MPa}$  and  $X_{Al}=25\text{wt.}\%$  (b)

The spring back of the compacts after ejection was also studied, which is characterized by the residual elasticity and expressed as  $R_e = [(l - l_0)/l_0] * 100\%$ , where  $R_e$  is the residual elasticity,  $l_0$  and  $l$  represent the length or diameter of the compact before and after ejection, respectively. The evolution of axial residual elasticity with the compaction pressure is shown in Fig. 10 (a), showing that  $R_e$  increases with  $P$ . Fig. 10 (b) displays the ejection force as a function of incremental modeling steps with each compaction pressure. At the beginning of the ejection, the ejection force must first conquer the maximum static friction force between the compact and the die wall, then the compact moves inside the die with the ejection force equal to the sliding friction force between the compact and the die wall, which shows an initial peak followed by a plateau in each curve. The larger the compaction pressure, the more significant difference between the maximum static friction force and sliding friction force, which can be clearly shown in the curve of  $P=300\text{MPa}$  in Fig. 10 (b). When part of the compact moves out of the die, the ejection force decreases nearly linearly, this is because the ejection force is proportional to the friction force between the die wall and the rest of compact inside the die. This process is similar to the physical and numerical results of some metallic and alloy powder ejection [44-46].

#### 4. Conclusions

FEM numerical simulation on the compaction of Fe and Al composite powders subjected to single action die compaction was carried out to systematically study the effects of Al powder content and compaction pressure on the relative density distribution, stress distribution. Meanwhile, the powder flow behavior, ejection process and

subsequent spring back were analyzed. The following conclusions can be drawn.

With each fixed compaction pressure, higher relative density of the compact can be obtained when the Al powder content is increased. And the dense packing area close to the upper corner of the compact increases, while the loose packing area close to the lower corner of the compact decreases. In this case, the relative density distribution get better. With fixed Al powder content (e.g. 25wt.%), larger dense or loose area close to the upper or lower corner of the compact can be identified when the compaction pressure is low. However, with the increase of the compaction pressure, the loose packing area at the lower corner of the compact decreases, which makes the relative density distribution uniform.

Accordingly, large and small equivalent Von Mises stresses appear at the upper and lower corner of the compact for each Al powder content, respectively. And with the increase of the compaction pressure, the value of the equivalent Von Mises stress and corresponding area at the upper corner of the compact increase, where the stress concentration can be identified. The equivalent Von Mises stress varies with the compaction pressure and Al powder content, and it increases with the former and decreases with the latter. During ejection, the ejection force is determined by the compaction pressure, the larger the compaction pressure, the higher the ejection force is needed, which will lead to larger spring back and stress redistribution after ejection.

Due to the die wall friction, the axial displacement at the central part of the compact is larger than that at the die wall, while the radial displacement indicates the convective powder flow behavior during compaction.

### Acknowledgements

We are grateful to the financial support of National Natural Science Foundation of China (No. 51374070) and Fundamental research funds for the Central Universities of China (N120202001).

### References

- [1] P. S. Liu, B. Yu, A. M. Hu et al., *J. Mater. Sci. Technol.*, 18 (2002) 299-305.
- [2] R. S. Sundar, D. H. Sastry, Y. V. R. K. Prasad, *Mat. Sci. Eng. A*, 347 (2003) 86-92.
- [3] F. Q. Lang, Z. M. Yu, S. Gedevarishvili, *Intermetallics*, 11 (2003) 135-141.
- [4] F. Q. Lang, Z. M. Yu, Gedevarishvili, et al., *Intermetallics*, 12 (2004) 469-475.
- [5] T. Sleboda, J. Kane, R. N. Wright, et al., *Mat. Sci. Eng. A*, 368 (2004) 332-336.
- [6] H. Z. Kang, C. T. Hu, *Mater. Chem. Phys.*, 88 (2004) 264-272.
- [7] E. Godlewska, S. Szczepanik, R. Mania, et al., *Intermetallics*, 11 (2003) 307-312.
- [8] A. Bouayada, C. Gerometta, A. Belkebir, et al., *Mat. Sci. Eng. A*, 363 (2003) 53-61.
- [9] V. K. Sikka, U. D. Wilkening, J. Liebetau, et al., *Mat. Sci. Eng. A*, 258 (1998) 229-235.
- [10] H. R. Shahverdi, M. R. Ghomashchi, S. Shabestar, et al., *J. Mater. Process. Tech.*, 258 (1998) 229-235.
- [11] D. L. Joslin, D. S. Easton, C. T. Liu, et al., *Mat. Sci. Eng. A*, 192 (1995) 544-548.
- [12] P. Z. Shen, M. Song, H. Y. Gao, et al., *J. Mater. Sci.*, 44 (2009) 4413-4421.
- [13] H. Y. Gao, Y. H. He, P. Z. Shen, et al., *Powder. Metall.*, 12 (2004) 469-475.
- [14] X. Z. An, Z. T. Xing, C. C. Jia, *Metall. Mater. Trans. A.*, 45 (2014) 2171-2179.
- [15] X. Z. An, Y. L. Zhang, Y. X. Zhang, S. Yang, *Metall. Mater. Trans. A*, 2015 (submitted).
- [16] T. Sinha, R. Bharadwaj, *Powder Technol.*, 202 (2010) 46-54.
- [17] K. A. Kuhn, C. L. Downey, *Int. J. Powder. Metall.*, 7 (1971) 15-25.
- [18] R. J. Green, *Int. J. Mech. Sci.*, 14 (1972) 215-224.
- [19] S. Shima, M. Oyane, *Int. J. Mech. Sci.*, 18 (1976) 285-291.
- [20] A. L. Gurson, *J. Eng. Mater-T. Asme.*, 99 (1977) 2-5.
- [21] S. M. Domivvelu, H. L. Gegel, I. S. Gunasekera, *Int. J. Mech. Sci.*, 26 (1984) 527-535.
- [22] A. K. Eksi, A. H. Yuzbasioglu, *Mater. Design*, 28 (2007) 1364-1368.
- [23] A. R. Khoei, A. R. Azami, S. Azizi, *J. Mater. Process. Tech.*, 185 (2007) 166-172.
- [24] K. Biswas, *J. Mater. Process. Tech.*, 166 (2005) 107-115.
- [25] S. M. Tahir, A. K. Ariffin, M. S. Anuar, *Adv. Powder. Technol.*, 202 (2010) 162-170.
- [26] H. Diarra, V. Mazel, V. Busignies, *Int. J. Pharmaceut.*, 453 (2013) 389-394.
- [27] Y. X. Zhang, X. Z. An, L. Y. Zhang, *Appl. Phys. A*, 118 (2015) 1015-1021.
- [28] W. Wu, G. Jiang, R. H. Wagoner, G. S. Daehn, *Acta Mater.*, 48 (2000) 4323-4330.
- [29] Y. Morimoto, T. Hayashi, T. Takei, *Int. J. Powder. Metall.*, 18 (1982) 129-145.
- [30] R. W. Lewis, A. G. K. Jinka, D. T. Gethin, *Int. J. Powder. Metall.*, 25 (1993) 287-293.
- [31] I. Aydin, B. J. Briscoe, K. Y. Sanliturk, *Comp. Mater. Sci.*, 3 (1994) 55-68.
- [32] A. R. Khoei, *Mater. Design*, 23 (2002) 523-529.
- [33] K. T. Kim, J. H. Cho, *J. Eng. Mater-T. Asme.*, 122 (2000) 119-128.
- [34] K. T. Kim, J. H. Cho, *Int. J. Mech. Sci.*, 43 (2001) 2929-2946.
- [35] M. F. Moreno, C. J. R. González Oliver, *Powder. Technol.*, 206 (2011) 297-305.
- [36] G. D. McAdam, *J. Iron. Steel. Inst.*, 168 (1951) 346-358.
- [37] N. A. Fleck, L. T. Kuhn, R. M. McMeeking, *J. Mech. Phys. Solids*, 40 (1992) 1139-1162.
- [38] A. R. Khoei, A. Bakhshiani, M. Mofid, *Finite Elem. Anal. Des.*, 40 (2003) 187-211.
- [39] A. R. Khoei, M. Mofid, A. Bakhshiani, *J. Mater. Process. Tech.*, 130 (2002) 175-180.
- [40] H. A. Haggblad, *Adv. Powder Technol.*, 67 (1991) 127-136.
- [41] G. M. Zhdanovich, V. A. Sidorov, C. A. Yakubovskii, *Powder Metall. Met. C+*, 6 (1982) 441-446.
- [42] A. Donev, S. Torquato, F. H. Stillinger, R. Connelly, *J. Appl. Phys.*, 95 (2004) 989-999.
- [43] Y. Y. Foo, Y. Sheng, B. J. Briscoe, *Int. J. Solids Struct.*, 41 (2004) 5929-5943.
- [44] R. Zhou, L. H. Zhang, B. Y. He, *Trans. Nonferrous Met. Soc. China.*, 23 (2013) 2374-2382.
- [45] D. T. Gethin, A. K. Arifin, D. V. Tran, et al., *Powder Metall.*, 37 (1994) 42-52.
- [46] R. K. Enneti, A. Lusin, S. Kumar, et al. *Powder Technol.*, 233 (2013) 22-29.